A Physics-Based RTD Model Accounting for Space Charge and Phonon Scattering Effects

Daniel R. Celino, Adelcio M. de Souza, Caio L. M. P. Plazas, Regiane Ragi and Murilo A. Romero

Department of Electrical and Computer Engineering, University of São Paulo, EESC-USP, São Carlos, Brazil.
e-mails: daniel.celino@usp.br and murilo.romero@usp.br

***Abstract*— This paper presents a fully analytical model for the current-voltage (I–V) characteristics of Resonant Tunneling Diodes. Based on Tsu-Esaki formalism, we consider the full electrical potential distribution in the structure, including the space charge regions at the emitter and collector layers. In addition, we account for the scattering suffered by carriers when tunneling through the double-barrier region, as a function of the applied bias voltage. These considerations improve the accuracy of the proposed model when compared with other approaches while keeping it physics-based and fully analytical. Finally, the model is validated with experimental and numerical data, demonstrating its feasibility for applications in circuit simulation environments.**

***Index Terms*— Physics-Based Model, Analytical Modelling, Resonant Tunneling Diode, TCAD Simulation.**

I. Introduction

In 1957, Leo Esaki (Physics Nobel Prize, 1973) named the tunnel diode based on an unusual physical phenomenon, the Negative Differential Resistance (NDR), arising from the inter-band tunneling process in p-n junctions [1]. Later, in 1964, Yogansen theoretically investigated the possibility of resonant quantum tunneling in double-barrier structures composed of layers of dielectrics in a metallic conductor [2]. Then, in 1969, Esaki and Tsu [3]-[4] proposed an artificial superlattice formed by the successive deposition of alternating semiconductor layers. In their paper [4], the authors demonstrated that the resulting current-voltage (**I–V**) characteristics display an NDR similar to that of tunnel diodes, although, in this case, due to intra-band resonant tunneling.

During the 1970s, progress in epitaxial growth techniques allowed the fabrication of double-barrier Resonant Tunneling Diodes (RTDs), where the quantum well region has a width comparable to the de Broglie wavelength. In the following decades, substantial improvements in the semiconductor industry technology allowed the enhancement of the Peak-to-Valley-Current-Ratio (PVCR) of the current density at room temperature, an important figure of merit for many RTD applications [5].

The RTD has always attracted attention from the research community, since the device is considered a promising candidate for both analog and digital applications due to its NDR intrinsic characteristic, high switching speed, and flexible design requirements [5]. More recently, several RTD applications in high-speed analog electronic circuits have been proposed, including the use of RTDs in the millimeter and sub-millimeter wave regimes [6]-[8]. In fact, the record for the highest oscillation frequency to date in an electronic circuit was experimentally verified when a RTD oscillator reached 1.92 THz [7]. The device has demonstrated solid performance as a resonator throughout in the THz frequency range, with high output powers [8], as RTD oscillators become solid candidates to integrate Sixth Generation (6G) mobile communications transceivers [9].

On the digital front, RTDs may be combined with silicon transistors to extend the performance of current technologies by increasing the switching speed while decreasing energy dissipation [10]. They are also useful in a wide range of novel applications, as digital circuits based on more than 2 bits logic [11]. In the low-temperature regime, the RTD has been investigated within the scope of spintronics. Spintronics offers the possibility of high-speed devices with low energy dissipation, enabling the combination between logic and memory devices [12]. The integration of spintronics and electronics can bring significant technology improvements, especially considering solutions based on spin polarization in non-magnetic RTDs [13]-[15].

Due to this diversity of applications, there is an ongoing effort to develop accurate RTD device models [5]. Among the available formalisms, one can mention the Non-Equilibrium Green's Functions (NEGFs) [16] and Wigner's transport equations [17]. Although very accurate, these numerical models require huge computing power and are not suitable for fast evaluations in the electronics industry, where it is necessary to simulate thousands of components simultaneously. On the other hand, compact models are an indispensable bridge between the device manufacturing process and the integrated circuit design. They provide simple mathematical expressions to accurately reproduce the device characteristics while keeping computational effort to a minimum.

In this framework, despite being a well-established device, the availability of RTD analytical models is very limited and there is no model available in the literature fully incorporating effects such as space charge formation and phonon scattering. Aiming to fulfill this niche, we develop an analytical compact model to describe the **I–V** characteristics of RTDs. including space-charge and phonon scattering mechanisms. This paper extends our previous work [18] with a more detailed model description and now includes an improved analytical expression to account for the longitudinal optical phonon (LO-phonon) effects. Also, we extended the model validation, by using the Silvaco TCAD package to evaluate the model accuracy regarding the variation of several physical and geometric parameters.

This paper is organized as follows: Section II. presents the required theoretical background and literature review. Next, in Section III., we outlined the proposed model, highlight-

Digital Object Identifier 10.29292/jics.v17il.545

ing our contributions. Then, in Section IV., we validate our model with data from three different devices described in the literature as well as several TCAD simulations, carrying out an in-depth discussion regarding the distinct features of the RTD **I–V** characteristics. Finally, in Section V., we draw the conclusions.

II. Background

A typical schematic of the RTD semiconductor layers is depicted in Fig. (1). As it can be seen, the RTD layer structure is composed by the emitter and the collector regions, typically heavily doped layers, and an undoped active region, which comprises the quantum well and the potential barriers. Usually, to reduce Coulomb scattering, undoped/low-doped spacer layers are also incorporated within the layer sequence, resulting in a higher PVCR [19]-[21].

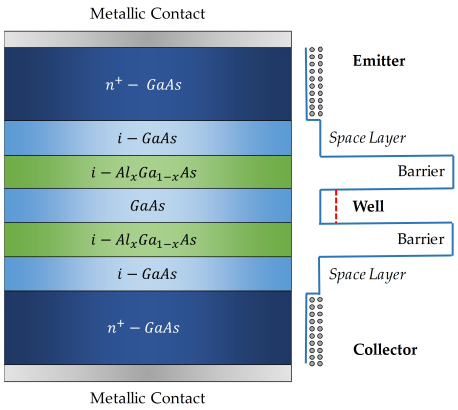

Fig. 1: Schematic illustration of a typical GaAs/AlGaAs Resonant Tunneling Diode layer sequence. Also shown it is a schematic illustration of the conduction band profile.

The standard model for RTDs is based on the pioneering carrier transport formalism proposed by R. Tsu and L. Esaki [22]. In this formalism, coherent electron transport is considered, i.e., the electrons traverse the potential barriers without loss of phase-coherence due to scattering mechanisms. Additionally, the following assumptions are made: the transverse momentum is conserved during the tunneling process; the electric field is uniformly distributed in the structure; the space charge regions are disregarded; the existence of charge sources or sinks throughout the structure is also ignored; the effective mass approximation is assumed the rectangular profile of the potential barriers is held even under an applied bias [22]-[23]. Under these assumptions, Tsu and Esaki derived the following current density expression:

$$J = \frac{em^* k_B T}{2\pi^2 \hbar^3} \int_0^\infty \mathbf{T}(E_x, V_a) \times \ln\left[\frac{1+\exp\left(\left(E_F - E_x\right)/k_B T\right)}{1+\exp\left(\left(E_F - E_x - eV_a\right)/k_B T\right)}\right] dE_x, \quad (1)$$

where e is the elementary charge, m^* is the effective mass of the electron, k_B is the Boltzmann's constant, T is the absolute temperature, $\hbar$ is the reduced Planck's constant, E_F is the Fermi energy level, V_a is the electrical bias potential applied to the structure, E_x is the longitudinal energy and $\mathbf{T}(E_x, V_a)$ is the tunneling transmission coefficient. The Tsu-Esaki model does not provide a close quantitative agreement with experimental **I–V** curves [5]. These discrepancies have been attributed to excessive simplifications, namely, the disregard of the inelastic scattering as well as space charge effects [24]. In particular, the formation of space-charge regions at the emitter and collector shifts the **I–V** peak position while the LO-phonon scattering degrades the PVCR.

To achieve a better agreement with measured data, it becomes necessary to modify the original Tsu-Esaki model to include previously overlooked physical effects [23]. As a result, a few analytical models have been proposed in the literature [5]. Several of those RTD models are behavioral models, suitable for SPICE simulations but not directly related to the physics of the device [26]. Just a few others can be considered physics-based models [25], [27]. However, even those physics-based models rely on semi-empirical fitting parameters, making it not possible to directly predict the relationship between the RTD geometry and layer structure and its electrical output characteristics. In this context, we address the lack of a fully physics-based RTD model. Specifically, in the following sections, we will present the development and validation of a RTD analytical model, incorporating a realistic potential distribution across the device, with the associated space charge effects, and considering phonon scattering mechanisms.

III. Model

A. Electric Potential Distribution Model

We start by considering the electric potential distribution in the set of distinct regions within the device. Namely, the potential drop in the accumulation region at the emitter layer, V_{acc}, in the double barrier region, V_{db} (comprising the summation of voltage drops at left barrier V_L, quantum well V_w and right barrier V_R) and in the depletion region at the collector layer V_d. Fig. (2) depicts a schematic illustration of the conduction band of the device under an applied bias voltage (V_a). Under an applied external bias, carriers are continuously removed from the accumulation region, by tunneling through the barriers, to the collector layer. The empty states in the accumulation region are occupied with electrons injected from the emitter contact. Thus, there is a steady supply of electrons contributing to the resonant tunneling current.

In realistic RTDs, space charge formation modifies the electric potential distribution in the structure, building up an accumulation region at the emitter layer and a depletion region at the collector layer. Depending on the width of the space layers and on the operational temperature, a quasi-triangular quantum well may form in the accumulation region at the emitter, yielding a two-dimensional electron gas (2-DEG) at the interface. In fact, the formation of this quantized region usually occurs in very low temperature regimes [15], [28]-[29]. In devices with quantized energy levels at the emitter layer, the resonant current density is commonly referred to as 2D-2D (concerning the nature of the emitter/well/collector density of states). However, for most applications at room temperature, the quantization may be ignored, and the resonant current density is considered as 3D-

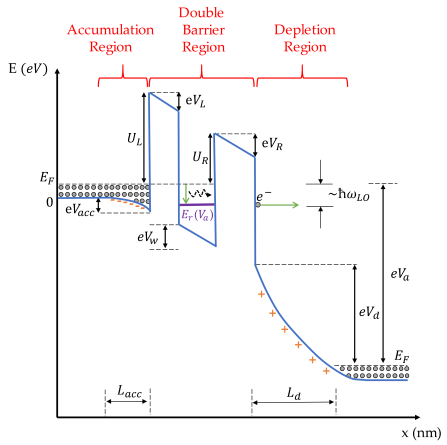

Fig. 2: Schematic illustration of the RTD conduction band profile under an applied external bias voltage V_a.

2D. Our specific **I–V** model for the 2D-2D case can be found elsewhere [30].

As proposed by Sheard and Toombs [31], under an applied bias voltage, the RTD can be modeled as two parallel-plate capacitors in series, with a negative charge $-Q_e$ at the emitter, a positive charge Q_c at the collector and a negative charge $-Q_w$ at the center plate, representing the well. In this picture, to meet the charge neutrality condition: $Q_c = Q_e + Q_w$. Also, as demonstrated by [31], the charge accumulation in the rectangular quantum well is balanced accordingly to the relation $Q_w \propto T_L/(T_L + T_R)$, where T_L and T_R are the single barrier transmission coefficients, relative to the left and right barriers, respectively. Hence, if the barrier widths are narrow, one can assume $Q_w \ll Q_e$ when out of resonance. Then, as a first approximation, in our model, we can neglect the charge storage in the well.

To determine the voltage drop in the accumulation region at the emitter side, we assume an uniform charge density as a function of the applied voltage $\rho_e(V_a)$. Then, the Poisson equation is $\nabla^2 V_e(x) = e\rho_e/(\kappa_e\epsilon_0)$, where κ_e is the emitter dielectric constant. The electric field in the emitter is $F_e(x) = -\nabla V_e(x)$, where the origin, $x = 0$, is placed at the left-hand side of the left barrier. Applying the usual boundary conditions, i.e., imposing $V_e(0) = 0$ and considering $F_e(-L_{acc}) = 0$ (the electric field vanishes in the neutral zone), the electric potential is

$$V_e(x) = \frac{e\rho_e}{2\kappa_e\epsilon_0} x(x + 2L_{acc}), \quad -L_{acc} \leq x \leq 0. \tag{2}$$

Hence, the voltage drop in the accumulation region is

$$V_{acc} = V_e(0) - V_e(-L_{acc}) = \frac{e\rho_e L_{acc}^2}{2\epsilon_e}.$$

The electric field at the interface between the accumulation region and the left potential barrier is $F_e(0) = e\rho_e L_{acc}/(\epsilon_0\kappa_e)$. Using the continuity of the electric displacement vector $\mathbf{D} = \epsilon\mathbf{F}$ at the interfaces between the well and the barriers, and knowing that the voltage drop over the potential double barrier region is given by $V_{db} = V_L + V_w + V_R$, we have

$$V_{db} = \frac{e\rho_e L_{acc} L_{bL}}{\kappa_b\epsilon_0} + \frac{e\rho_e L_{acc} L_w}{\kappa_w\epsilon_0} + \frac{e\rho_e L_{acc} L_{bR}}{\kappa_b\epsilon_0}, \tag{3}$$

where κ_b and κ_w are the dielectric constants in the barrier and in the well, respectively. The terms L_{bL} and L_{bR} are the widths of the left and right potential barriers, respectively. The term L_w refers to the width of the rectangular quantum well (see Fig. (2)). From the charge neutrality principle, considering $Q_w \approx 0$, we have $Q_e \simeq Q_c$, leading to $\rho_e L_{acc} A = \rho_c L_d A$, where A is cross-section area of the device. Thus, the depletion width is $L_d = (\rho_e/\rho_c)L_{acc}$. For the depletion width at the collector side, we consider the total depletion approximation, with $\rho_c = |e|\, N_d$, where N_d is the effective doping concentration at the collector layer. Thus, the voltage drop over the depletion region is given by

$$V_d = \frac{eN_d L_d^2}{2\kappa_c\epsilon_0} = \frac{e\rho_e^2 L_{acc}^2}{2\kappa_c\epsilon_0 N_d}.$$

For high doping levels, the effect of electrostatic screening in the semiconductor layer becomes relevant. Therefore, in this work, the approximate accumulation width is obtained using the Thomas-Fermi screening theory [31]:

$$L_{acc} = \left(\frac{\kappa_c\epsilon_0\hbar^2 \sqrt[3]{\pi^4}}{e^2 m_e^* \sqrt[3]{3N_d}} \right)^{\frac{1}{2}}. \tag{4}$$

By inspecting the band diagram in Fig. (2), the following relation is obtained:

$$V_a = V_{acc} + V_{db} + V_d. \tag{5}$$

Replacing each respective voltage drop term for their expression as a function of the electron concentration at the emitter, we have:

$$V_a = a_1\rho_e + a_2\rho_e^2, \tag{6}$$

where

$$a_1 = \frac{eL_{acc}}{\epsilon_0}\left[\frac{L_{acc}}{2\kappa_e} + \frac{(L_{bL} + L_{bR})}{\kappa_b} + \frac{L_w}{\kappa_w}\right]$$

$$a_2 = \frac{eL_{acc}^2}{2\epsilon_c N_d}.$$

Solving Eq. (6) and choosing the positive root:

$$\rho_e(V_a) = -\frac{1}{2a_2}\left(a_1 - \sqrt{a_1^2 + 4a_2 V_a}\right). \tag{7}$$

From the value of $\rho_e(V_a)$, it is possible to analytically compute each term of the voltage drop in the RTD, as a function of the applied voltage.

B. Tunneling Transmission Coefficient

One of the leading causes for the loss of phase coherence in RTDs is the scattering by LO-phonons [32]-[33]. It occurs even in the state-of-the-art RTDs, since the electron relaxation time due to scattering of LO-phonons is much shorter than the dwell time. To account for the electron-phonon interactions, we use the expression proposed by Büttiker [34], derived to include inelastic scattering effects in a global coherent tunneling framework. In addition, this approach takes into account unequal potential barrier heights,improving the accuracy of the model. The Büttiker's expression is given as

$$\mathbf{T}_n(E,V_a) = \frac{\Gamma_L\Gamma_R}{(\Gamma_L+\Gamma_R)}\left(\frac{\Gamma_T}{\Gamma_T^2/4+(E-E_n(V_a))^2}\right), \tag{8}$$

where $E_n(V_a)$ is the energy level in the well, expressed as a function of applied voltage and Γ_L and Γ_R are the left and right barrier intrinsic resonance linewidths, respectively. The term Γ_T refers to the total resonance linewidth given by $\Gamma_T = \Gamma_L+\Gamma_R+\Gamma_s$ where Γ_s is the linewidth due to scattering by LO-phonons. From Heisenberg uncertainty principle, one can write $\Gamma_s \approx \hbar/\tau_s$, where τ_s is the momentum relaxation time. The left and right intrinsic resonance linewidths are $\Gamma_{L,\,R} = v_w\,(2L_w)^{-1}\,\hbar T_{L,\,R}(E,V_a)$, with the electron velocity in the well given by $v_w = \sqrt{2E_n/m_w^*}$ [34].

In our proposed model, we used the well-known WKB approximation to calculate the tunneling transmission coefficient for the case of a single potential barrier. To improve accuracy, when compared to other models in the literature, $T_{L,\,R}$ is also written as a function of the applied bias. Therefore:

$$\begin{aligned} T_{L,R}(E,V_a) \;=\; & \left|\exp\left(-\frac{4L_{bL,bR}\sqrt{2m_b^*}}{3\hbar eV_{L,R}}\left[(U_{L,R}(V_a))^{3/2}\right.\right.\right. \\ & \left.\left.\left.-\,(U_{L,R}(V_a)-eV_{L,R})^{3/2}\right]\right)\right|. \end{aligned} \tag{9}$$

From Fig. (2), under an applied bias, the effective left-barrier height for a electron with an incident energy $E = E_F$ is $U_L(V_a) = U_0 - E_F - eV_{acc}$ and the effective right-barrier height under the same conditions is $U_R(V_a) = U_L(V_a) - eV_L - eV_w$, where U_0 is the barrier height in absence of an applied bias. As proposed by Mizuta *et al.* [35], the momentum relaxation time is calculated by the expression [37]:

$$\begin{aligned} \frac{1}{\tau_s} &= \alpha_F\omega_{LO}\left(\frac{\hbar\omega_{LO}}{E_n}\right)^{1/2} \\ &\quad\times N_{\mathbf{g}}\left\{\ln\left|\frac{a_{LO}+1}{a_{LO}-1}\right| + \exp\left(\frac{\Theta}{T}\right)\ln\left|\frac{1+b_{LO}}{1-b_{LO}}\right|\right\}, \end{aligned} \tag{10}$$

where $\hbar\omega_{LO}$ is the phonon energy and α_F is the Fröhlich polar constant:

$$\alpha_F = \frac{e^2\sqrt{m_w^*}}{4\sqrt{2}\pi\epsilon_0\hbar\sqrt{\hbar\omega_{LO}}}\left(\frac{1}{\kappa_\infty}-\frac{1}{\kappa_0}\right), \tag{11}$$

where κ_∞ and κ_0 are the high frequency and static dielectric constants, respectively [36]. The parameter $N_{\mathbf{g}}$ is the average number of phonons in the g mode, as described by the Bose-Einstein thermal distribution [37], $N_{\mathbf{g}} = (\exp(\Theta/T)-1)^{-1}$. The a_{LO} and b_{LO} parameters are defined as

$$a_{LO} = \left(1+\frac{\hbar\omega_{LO}}{E_n}\right)^{1/2},\; b_{LO} = Re\left(1-\frac{\hbar\omega_{LO}}{E_n}\right)^{1/2}.$$

The term Θ refers to the Debye temperature, which can be calculated as $\Theta = \hbar\omega_{LO}/k_B$ [36]-[37]. As demonstrated in [35], the proposed approximation for Γ_s shows a good agreement with experimental data.

C. Current Model

In our approach, to derive a fully analytical model, it is necessary to analytically compute the energy levels in the quantum well. For this region, the potential profile is simply $U(x) = 0$ inside of the well and $U(x) = U_0$ outside. As usual, in the effective mass approximation, the Schrödinger's equation is given by $\hat{\mathbf{H}}\Psi(x) = E_n\Psi(x)$, where the Hamiltonian operator is $\hat{\mathbf{H}} = -\hbar^2\nabla^2/(2m^*)+U(x)$. In contrast with the infinite quantum well problem, which has an exact analytical solution, the finite-well case depends on finding the roots of transcendental equations, which are usually solved by numerical routines. Alternatively, in our model, the resonant energy levels under equilibrium $E_n(0)$ are computed analytically. Also, to improve accuracy and unlike most formulations, we consider the difference between the effective masses of the barriers and well layers. The detailed model to calculate the energy levels can be found in [38]. It is worth mentioning that our analytical expressions provide an agreement greater of about 99% for most practical cases in micro and nanoelectronics.

In order to achieve a compact model for RTD I-V characteristics, the transmission coefficient is taken as negligible, except around resonance, when the electron kinetic energy E_x is close to the energy levels in the well E_n [25]. Hence, under an external applied voltage, we approximate:

$$E_x \approx E_n(V_a) = E_n(0) - eV_{acc} - eV_L - eV_w/2 \tag{12}$$

Accordingly, the logarithmic part of Eq. (1) can be pulled out of the integral. In addition, if one replaces the term $\mathbf{T}(E_x,V_a)$ in Eq. (1) by the Büttiker's approximation, given by Eq. (8), replace E_x in the the logarithmic part of Eq. (1) by Eq. (12), and integrate Eq. (1) from 0 up to ∞, the generalized RTD current becomes

$$\begin{aligned} I(V_a) \;=\; & \frac{em_\parallel^* k_BTA}{\pi^2\hbar^3}\left(\frac{\Gamma_L\Gamma_R}{\Gamma_L+\Gamma_R}\right)\sum_n \\ & \ln\left[\frac{1+\exp\left(\left(E_F-E_n(V_a)\right)/k_BT\right)}{1+\exp\left(\left(E_F-E_n(V_a)-eV_a\right)/k_BT\right)}\right] \\ & \times\left[\frac{\pi}{2}+\arctan\left(\frac{E_n(V_a)}{\Gamma_T/2}\right)\right], \end{aligned} \tag{13}$$

where summation accounts for the all allowed energy levels in the quantum well.

IV. Validation Results

To validate our model, we compare our results, obtained by means of Eq. (13) with experimental and numerical data extracted from several different RTD structures described in the literature. The electron effective masses and the dielectric constants in GaAs, AlAs and $Al_xGa_{1-x}As$, the theoretical LO-phonon energy value, $\hbar\omega_{LO}$, as well the theoretical value of U_0, are obtained from [36], [39].

RTD #1

We start validating our model with the device described in [25]. RTD #1 is composed of an $In_{0.53}Ga_{0.47}As$/AlAs heterostructure with $L_{bL} = L_{bR} = 2.6nm$ and $L_w = 4.8\ nm$. The operating temperature is $T = 300K$, the nominal donor doping level is $N_d = 1 \times 10^{18} cm^{-3}$and the Fermi level position is around $E_F \approx 50\ meV$. As it can be seen from Fig. (3), the proposed model provides very good agreement with the measured curve, correctly describing the resonance peak as well as the magnitude of the current density experimentally obtained. In order to achieve this agreement, we replaced the parameter ρ_e by $\rho'_e = \alpha\rho_e$, where α is a fitting parameter. This fitting parameter is justified because, in realistic devices, the accumulation width L_{acc} also varies with the applied bias. For RTD #1, we set $\alpha = 0.5$. Also, the barrier width used in our simulation was set to $2.55nm$, a small adjustment in the order of a few Bohr's radii, within the uncertainty range of the usual epitaxial growth techniques. Finally, we point out that the shoulder-like shape observed in the experimental curve in Fig. (3) is an unwanted feature attributed to the non-ideal effects of intrinsic bistability and feedback which are sometimes present in fabricated devices [5], [31]. Those non-idealities are not included in our compact model.

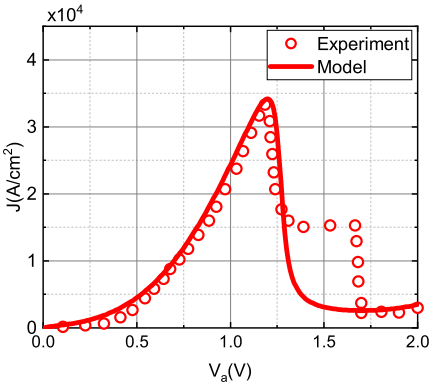

Fig. 3: Comparison between the **I–V** curves obtained by the proposed current density model (solid curve) and experimental data (symbols) of the RTD described in [25].

RTD #2

The second device considered is the RTD investigated by Yang et al. [40], composed of a GaAs/AlAs heterostructure, with $L_{bL} = L_{bR} = 1.7nm$ and $L_w = 4.5\ nm$. For this RTD: $T = 300K$, $N_d = 1 \times 10^{18} cm^{-3}$ and $E_F \approx 60\ meV$. Fig. (4) shows the analytical and the experimental **I–V** curves. Our model provides a good agreement with the experimental data, correctly describing the I-V characteristic of the device, including the location of the resonance peak, and the magnitude of the current density. Again, to achieve this result, a small adjustment in some nominal parameters were necessary. Namely, $N_d = 0.85 \times 10^{18} cm^{-3}$, $L_w = 4.3\ nm$, $L_{bL} = L_{bR} = 1.55nm$ and $\alpha = 0.5$. The minor differences are because the GaAs/AlAs heterostructure has an indirect bandgap, leading to an additional broadening in total resonance linewidth. In our model, we neglect the contribution of tunneling carriers due to other channels, such as the inter-band tunneling from $\Gamma - X$ and $\Gamma - L$ bands. As a consequence, the valley current measured in this case is greater than the theoretical value predicted by our proposed model. Nevertheless, even for the indirect bandgap condition, our model closely matches the experimental curve, with minimal adjustments in the nominal parameters. Also, our model correctly describes the position of peak and valley regions.

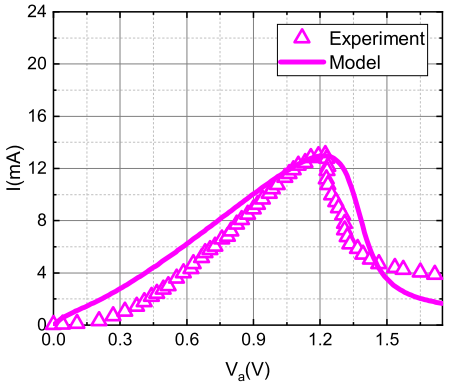

Fig. 4: Comparison between the **I–V** curves obtained by the proposed current density model (solid curve) and the experimental data (symbols) of the RTD reported in [40].

RTD #3

RTD #3 is composed by a $Al_{0.33}Ga_{0.67}As$/GaAs heterostructure with $L_{bL} = L_{bR} = 3.0nm$ and $L_w = 3.0\ nm$, numerically studied by [41]. For this device, we have $T = 77K$, $N_d = 1 \times 10^{18} cm^{-3}$ and $E_F \approx 54\ meV$. As it can be seen in Fig. (5), the proposed model provides an excellent agreement with the self-consistent numerical calculations. Indeed, the model can predict the peak position, the peak magnitude, the resonance width, achieving a close agreement for the value of the PVCR. Once again, a small adjustment in some nominal parameters, well within the expected range of experimental variation in growth process, was necessary: $\alpha = 1.0$, $L_{bL} = L_{bR} = 2.8nm$ and $N_d = 1.2 \times 10^{18} cm^{-3}$.

RTD #4

RTD #4 is a device configured by ourselves, using the Silvaco Atlas TCAD software. It is composed of an $Al_{0.5}Ga_{0.5}As$/GaAs heterostructure with $L_{bL} = L_{bR} = 2.0nm$, $L_w = 2.5\ nm$. The contact regions, emitter and collector, are composed of 40-nm width, heavily doped GaAs layers with $N_d = 1 \times 10^{18} cm^{-3}$ followed by an undoped space layer of $7\ nm$ width. For this device, $T = 300K$ and $E_F \approx 55\ meV$. As it can be seen from Fig. (5), the proposed model provides a very close agreement to the simulated result, which is based on a self-consistent electric potential model and the NEGF carrier transport formalism. To achieve this agreement, we used $\alpha = 1.2$ in our calculations.

Fig. (7-a) shows the electronic concentration at the resonant peak ($V_a = 0.5\ V$) while Fig. (7-b) shows the electronic concentration at valley region ($V_a = 0.8\ V$). The results ob-

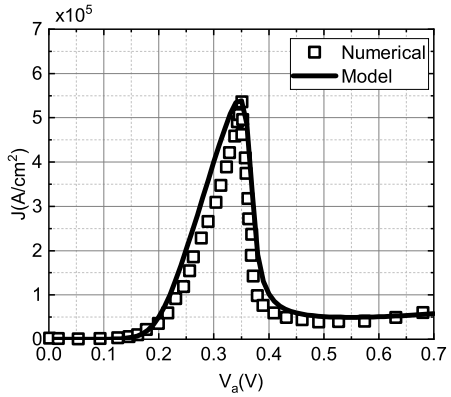

Fig. 5: Comparison between the **I–V** curves obtained by the proposed current density model (solid curve) and the self-consistent numerical simulation (symbols) reported in [41].

tained through our model are consistent with the numerical results arising from the TCAD simulation. From Fig. (7) one can see that, at the resonance peak, the electronic concentration in the quantum well reaches its maximum value, while at the valley voltage range, the electronic concentration in the well is significantly reduced, reinforcing our previous assumption that $Q_w \ll Q_e$ when out of resonance.

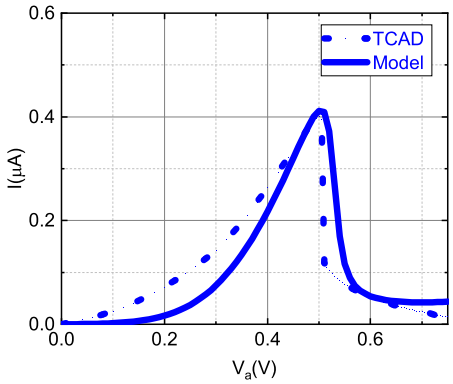

Fig. 6: Comparison between the **I–V** curves obtained by the proposed current density model (solid curve) and the quantum transport numerical simulation (doted curve) carried out using the Atlas Silvaco TCAD software.

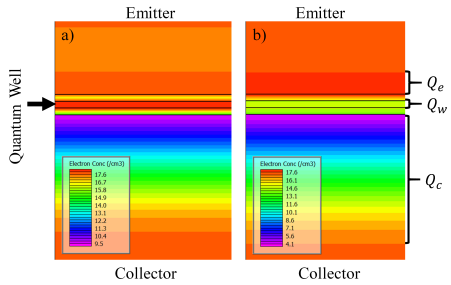

Fig. 7: Simulated 2D maps of the charge density for RTD #4. a) electronic concentration at the resonance peak. b) electronic concentration at the valley voltage range. The color change within the quantum well, from red to green, indicates a variation in the charge concentration, of about three orders of magnitude.

RTD #5

Again, RTD #5 is a device configured using Silvaco Atlas TCAD software. This RTD is composed by a $Al_{0.4}Ga_{0.6}As/GaAs$ heterostructure with $L_{bL} = L_{bR} = 2.5nm$, simulated for three different well widths, L_w,of $2.0, 2.5$ and 3.0 nm,respectively. Outside the active region, for the access contact regions, we emulated fabricated RTDs, in such way that a heavily doped layer ($n^{++} = 1 \times 10^{18} cm^{-3}$) with $0.1\mu m$ width followed by a lightly doped region ($n^{+} = 1 \times 10^{16} cm^{-3}$) with 50 nm width are used. In addition, to reduce Coulomb scattering, we included a 2.5 nm undoped space layer, separating the double-barriers/quantum-well active region from the contacts. For this device, $E_F \approx 48$ meV at $T = 300K$. As it can be seen from Fig. (5), the proposed model provides a close agreement with the simulated results for values of L_w. To achieve such an agreement, we used $N_d = 0.92 \times 10^{18} cm^{-3}$ and $\alpha = 1.05$ in our calculations.

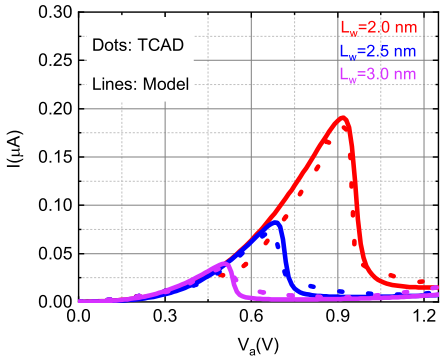

Fig. 8: Comparison between the **I–V** curves provided by the proposed current density model (solid curve) and the quantum transport numerical simulation (doted curve) obtained by TCAD simulation, for RTD #5, as a function of the well width L_w.

RTD #6

RTD #6 is also another device configured using Silvaco Atlas TCAD software. It is composed of an $Al_{0.4}Ga_{0.6}As/GaAs$ heterostructure with $L_{bL} = L_{bR} = 2.5nm$ and $L_w = 2.0nm$. For this device, for the contact regions, we again employed a heavily doped layer ($n^{++} = 1 \times 10^{18} cm^{-3}$) with $0.1\mu m$ width followed by a lightly doped region ($n^{+} = 1 \times 10^{16} cm^{-3}$) with 50 nm width. We also included a 2.5 nm undoped space layer. The Fermi energy level is $E_F \approx 48$ meV at $T = 300K$. As it can be seen from Fig. (9-a), the proposed model provides a good agreement with the simulated results, correctly predicting the main features of the **I–V** curve. For this structure, we also contrasted our expression to compute the charge accumulated at the emitter region against the TCAD data. The emitter charge is given by $Q_e = \rho_e L_{acc} A$, where the charge density ρ_e is calculated using Eq. (7). As it can be seen in Fig. (9-b), our proposed solution gives a fair agreement with the TCAD results within the range of applied voltages. The TCAD results for Q_e deviate from our theoretical predictions around $V_a = 0.8$ V, i.e., around the resonance peak. This occurs because, at resonance, part of the charge accumulated at the emitter is transferred to the quantum well by tunneling through the left barrier. Hence, a decrease in the amount of charge at the accumulation region is expected. This effect is not predicted by our analytical model since we neglect the charge stored in the quantum well. Nevertheless, our model shows a good agreement with the simulated results with only minor adjustments in the nominal values:

$N_d = 0.94 \times 10^{18} cm^{-3}$, $L_{bL} = L_{bR} = 2.4nm$ and $\alpha = 1.11$.

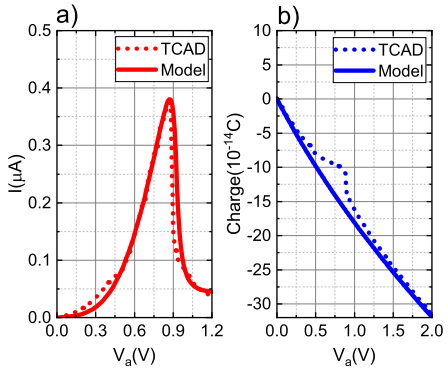

Fig. 9: Comparison between the results obtained by our proposed model (solid curves) and the TCAD simulation results (dotted curves) for RTD #6. a) **I–V** characteristics. b) emitter charge.

RTD #7

Finally, to further assess the accuracy of our model, we performed a TCAD investigation for an RTD employing an $Al_xGa_{1-x}As/GaAs$ heterostructure. The goal here is to evaluate the robustness of our model for two different values of alloy composition, $x = 0.3$ and $x = 0.5$, while keeping the remaining parameters unchanged. For this device, we set $L_{bL} = L_{bR} = 2.5nm$ and $L_w = 2.0nm$. RTD #7 is composed of a heavily doped region ($n^{++} = 1 \times 10^{18} cm^{-3}$) with $0.1\mu m$ width followed by a lightly doped region ($n^{+} = 1 \times 10^{16} cm^{-3}$) with $50\ nm$ width. Again, we include an undoped space layer with $2.5\ nm$ width to reduce Coulomb scattering. The Fermi energy level is $E_F \approx 48\ meV$ at $T = 300K$. As it can be seen from Figs. (10-a) and (10-b), the proposed model yields a good agreement with both simulated results, correctly predicting the main features of the **I–V** curves. To reach such an agreement, we performed minor adjustments on the nominal values of some parameters: $N_d = 0.88 \times 10^{18} cm^{-3}$ and $\alpha = 1.05$.

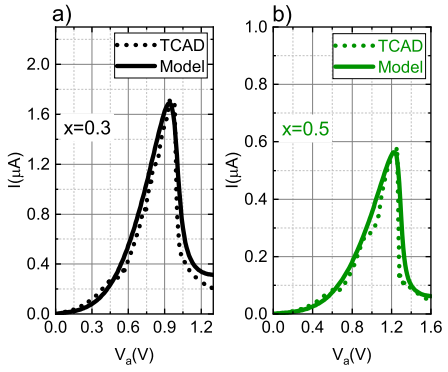

Fig. 10: Comparison between the **I–V** curves obtained by the proposed current density model (solid curve) and the TCAD simulation results (doted curve) for RTD #7. a) $x = 0.3$. b) $x = 0.5$.

V. Conclusion

In this paper, we developed a fully analytical compact model to describe the **I–V** characteristics of RTDs, on the basis of the Tsu-Esaki formalism. In order to improve accuracy, we computed the overall electric distribution in the RTD structure, including space charge build-up effects. The global tunneling coefficient is also calculated analytically, considering potential profile distribution in the whole structure, as well as the LO-phonon scattering mechanisms. To evaluate the resonant tunneling coefficient, we considered the asymmetry between potential barriers on the right and left sides of the quantum well, imposed by the external bias. Finally, we also employ an original method to analytically find the resonant energy levels in the quantum well, depending only on physical parameters. The proposed model was validated against experimental data available the literature and several numerical simulations performed by TCAD software, yielding excellent agreement.

Acknowledgments

The authors would like to thank the funding agencies CAPES, CNPq (Grant Number: 303708/2017-4), and Fapesp (Grant Number:18/13537-6) for their financial support.

References

[1] L. Esaki, “New phenomenon in narrow germanium p-n junctions,” *Phys. Rev.*, vol. 109, no. 2, pp. 603–604, Jan. 1958.

[2] L. V. Iogansen, “The Possibility of Resonance Transmission of Electrons in Crystals Through a System of Barriers,” *Sovt. Phys. J. Exptl. Theoret. Phys.*, vol. 18, no. 1, pp. 146-150, Jan. 1964.

[3] L. Esaki and R. Tsu, ”Superlattice and negative conductivity in semiconductors,” *IBM Research Note RC-2418*, Jan. 1969.

[4] L. Esaki and R. Tsu, “Superlattice and Negative Differential Conductivity in Semiconductors,” *IBM J. Res. Dev.*, vol. 14, no. 1, pp. 61-65, Jan. 1970.

[5] J. P. Sun, G. I. Haddad, P. Mazumder and J. N. Schulman, ”Resonant tunneling diodes: models and properties”, *Proc. IEEE*, vol. 86, no. 4, pp. 641–660, Apr. 1998.

[6] N. Oshima, K. Hashimoto, S. Suzuki and M. Asada, “Terahertz Wireless Data Transmission With Frequency and Polarization Division Multiplexing Using Resonant-Tunneling-Diode Oscillators,” *IEEE Trans. Terahertz Sci. Technol.*, vol. 7, no. 5, pp. 593–598, Sep. 2017.

[7] T. Maekawa, H. Kanaya, S. Suzuki, and M. Asada, “Oscillation up to 1.92 THz in resonant tunneling diode by reduced conduction loss” *Appl. Phys. Exp.*, vol. **9**, no. 2, p. 24101, Jan. 2016.

[8] E. Wasige *et al.*, “Resonant tunnelling diode terahertz sources for broadband wireless communications,” in *Terahertz, RF, Millimeter, and Submillimeter-Wave Technology and Applications X*, p. 101031J, Feb. 2017.

[9] P. Hillger *et al.*, “Toward Mobile Integrated Electronic Systems at THz Frequencies,” *J. Infrared, Millimeter, Terahertz Waves*, vol. 41, no. 7, pp. 846–869, Jul. 2020.

[10] S. Luryi, A. Zaslavsky “Blue sky in SOI: new opportunities for quantum and hot-electron devices” *Solid-State Electronics,* vol. 48, 877–885, Jun. 2004.

[11] H. C. Lin, “Resonant Tunneling Diodes For Multi-Valued Digital Applications” in *Proceedings IEEE Int. Symp. Multiple Valued Logic*, pp. 188–195, May 1994.

[12] D. D. Awschalom and M. E. Flatté, “Challenges for semiconductor spintronics,” *Nat. Phys.*, vol. 3, no. 3, pp. 153–159, Mar. 2007.

[13] H. B. de Carvalho *et al.*, “Voltage-controlled hole spin injection in nonmagnetic GaAs/AlAs resonant tunneling structures,” *Phys. Rev. B*, vol. 73, no. 15, p. 155317, Apr. 2006.

[14] L. F. dos Santos *et al.*, "Circular polarization in a non-magnetic resonant tunneling device," *Nanoscale Res. Lett.*, vol. 6, no. 1, p. 101, Dec. 2011.

[15] Y. Galvão Gobato *et al.*, "Spin injection from two-dimensional electron and hole gases in resonant tunneling diodes," *Appl. Phys. Lett.*, vol. 99, no. 23, p. 233507, Dec. 2011.

[16] R. Lake, G. Klimeck, R. C. Bowen, and D. Jovanovic, "Single and multiband modeling of quantum electron transport through layered semiconductor devices," *J. Appl. Phys.*, vol. 81, no. 12, pp. 7845–7869, Jun. 1997.

[17] J. Lee and M. Shin, "Quantum Transport Simulation of Nanowire Resonant Tunneling Diodes Based on a Wigner Function Model With Spatially Dependent Effective Masses", *IEEE Trans. on Nanotech.*, vol. 16, no. 6, pp. 1028-1036, Nov. 2017.

[18] D. R. Celino, A. M. de Souza, C. L. M. P. Plazas, R. Ragi and M. A. Romero, "Fully Analytical Compact Model for the I–V Characteristics of Resonant Tunneling Diodes", in *35^{th} Symposium on Microelectronics Technology*, pp. 1-4, Campinas-SP, Brazil, Aug. 2021.

[19] B. Gu, C. Coluzza, M. Mangiantini and A. Frova, "Scattering effects on resonant tunneling in double-barrier heterostructures," *Appl. Phys.,* vol. 65, p. 3510, Oct. 1989.

[20] M. A. Remnev, I. Y. Kateev and V. F. Elesin, "Effect of spacer layers on current-voltage characteristics of resonant-tunneling diode," *Semiconductors,* vol. 44, no. 8, pp. 1034–1039, Dec. 2010.

[21] I. Mehdi, R. K. Mains, and G. I. Haddad, "Effect of spacer layer thickness on the static characteristics of resonant tunneling diodes," *Appl. Phys. Lett.,* vol. 51, no. 9, Aug. 1990.

[22] R. Tsu e L. Esaki, "Tunneling in a finite superlattice", *Apply. Phys. Lett.*, vol. 22, no. 11, pp. 562-564, Mar. 1973.

[23] M. O. Vassell, Johnson Lee, and H. F. Lockwood. "Multibarrier tunneling in Ga1-xAlxAs/GaAs heterostructures". *J. Appl. Phys*., vol. 54, 5206, Jan. 1983.

[24] A. D. Stone and P. A. Lee, "Effect of Inelastic Processes on Resonant Tunneling in One Dimension", *Phys. Rev. Lett*., vol. 54, 1196, Mar. 1985.

[25] J. N. Schulman, H. J. De Los Santos and D. H. Chow, "Physics-based RTD current-voltage equation", *IEEE Electron Device Lett.*, vol. 17, no. 5, pp. 220-222, May 1996.

[26] E. R. Brown, O. B. McMahon, L. J. Mahoney and K.M. Molvar, "SPICE model of the resonant-tunnelling diode", *Electronic Letters*, vol. 32**,** no. 10, May 1996.

[27] S. L. Yadav and H. Najeeb-ud-din, "A simple analytical model for the resonant tunneling diode based on the transmission peak and scattering effect," *J. Comput. Electron.*, vol. 19, no. 3, pp. 1061–1067, Sep. 2020.

[28] T. Fiig, A.P. Jauho, "Self-consistent modelling of resonant tunnelling structures," *Surface Science*, vol. 267, pp. 392-395, Jul. 1992

[29] J. S. Wu *et al.,* "Resonant tunneling of electrons from quantized levels in the accumulation layer of double barrier heterostructures," *Appl. Phys.Lett.,* vol. 57, no. 26, p. 2311, Nov. 1990.

[30] D. R. Celino, R. Ragi and M. A. Romero, "An Analytical Physics-Based Model for the **I-V** Characteristics of 2D-2D RTDs," to be published.

[31] F. W. Sheard and G. A. Toombs, "Space-charge buildup and bistability in resonant-tunneling double-barrier structures," *Appl. Phys. Lett.*, vol. 52, no. 15, pp. 1228–1230, Apr. 1988..

[32] F. Chevoir and B. Vinter, "Calculation of phonon-assisted tunneling and valley current in a double-barrier diode," *Appl. Phys. Lett.*, vol. 55, no. 18, pp. 1859–1861, Oct. 1989.

[33] V. J. Goldman, D. C. Tsui, and J. E. Cunningham, "Evidence for LO-phonon-emission-assisted tunneling in double-barrier heterostructures," *Phys. Rev. B*, vol. 36, no. 14, pp. 7635–7637, Nov. 1987.

[34] M. Buttiker, "Coherent and sequential tunneling in series barriers," *IBM J. Res. Dev.*, vol. 32, no. 1, pp. 63–75, Jan. 1988.

[35] H. Mizuta, T. Tanoue and S. Takahashi, "Theoretical analysis of peak-to-valley ratio degradation caused by scattering processes in multi-barrier resonant tunneling diodes", in *Proceedings of IEEE/Cornell Conference on Advanced Concepts in High Speed Semiconductor Devices and Circuits*, pp. 274, Sep. 1989.

[36] S. Adachi, "GaAs, AlAs, and $Al_xGa_{1-x}As$: Material parameters for use in research and device applications," *J. of Appl. Phys.,* vol. 58, no. 3, pp. R1-R29, Aug. 1985.

[37] K. Seeger, Semiconductor Physics: An Introduction, 9th ed. Berlin: Springer Berlin Heidelberg, 2004.

[38] D. R. Celino, M. A. Romero, and R. Ragi, "Accurate and fully analytical expressions for quantum energy levels in finite potential wells for nanoelectronic compact modeling," *J. Comput. Electron.*, Oct. 2021.

[39] S. Adachi, "Material parameters of $In_{1-x}Ga_xAs_yP_{1-y}$ and related binaries," *J. Appl. Phys.,* vol. 53, no. 12, pp. 8775–8792, Dec. 1982.

[40] L. Yang, S. D. Draving, D. E. Mars, and M. R. T. Tan, "A 50 GHz broad-band monolithic GaAs/AlAs resonant tunneling diode trigger circuit," *IEEE J. Solid-State Circuits*, vol. 29, no. 5, pp. 585–595, May 1994.

[41] W. Pötz, "Self-consistent model of transport in quantum well tunneling structures," *J. Appl. Phys.*, vol. 66, no. 6, pp. 2458–2466, Sep. 1989..